

Nanoparticle Assembly at Fluid Interfaces: Structure and Dynamics

Yao Lin,[†] Alexander Böker,[†] Habib Skaff,[†] David Cookson,[‡] A. D. Dinsmore,^{*,§}
Todd Emrick,^{*,†} and Thomas P. Russell^{*,†}

Department of Polymer Science and Engineering, University of Massachusetts,
Amherst, Massachusetts 01003, Australian Nuclear Science and Technology Organization,
PMB 1, Menai 2234, Australia, and Department of Physics, University of Massachusetts,
Amherst, Massachusetts 01003

Received August 9, 2004. In Final Form: September 28, 2004

The self-assembly of nanoparticles at fluid interfaces, driven by the reduction in interfacial energy, was investigated. With spherical, tri-*n*-octyl-phosphine-oxide covered cadmium selenide (CdSe) nanoparticles (1–8 nm), thermal fluctuations compete with the interfacial segregation giving rise to a size-dependent self-assembly of the particles. The structure of the nanoparticle assembly was studied using electron microscopy, atomic force microscopy, and X-ray scattering in situ, which indicate that the particles form a densely packed monolayer. The energetics of the adsorption of nanoparticles onto the interface was revealed by time-dependent fluorescence studies on a mixture of two different sized nanoparticles at the interface. The dynamics of the nanoparticles at the fluid interface, probed using fluorescence photobleaching methods, suggests a liquid-like behavior. The results have implications in the design of hierarchical self-assemblies of nanoparticles for the one-step fabrication of devices on multiple length scales.

Introduction

As many top-down manufacturing methods approach practical limitations, the development of viable self-assembly processes that result in functional nanostructured materials grows in importance. The self-assembly of colloidal particles at fluid interfaces, driven by the reduction in interfacial energy, is well established.^{1,2} Interfaces between immiscible fluids, i.e., on the surface of droplets, are ideal for the assembly of micron-sized colloidal particles.^{3,4} Later studies^{5–9} have focused on the assembly of particles having a size less than 10 nm. Particles of this size scale are of interest owing to their unusual optoelectronic properties.^{10–15} Recently, the hi-

erarchical self-assembly of ligand-stabilized colloidal nanoparticles at fluid interfaces was reported,^{16,17} where thermal fluctuations, in competition with interfacial energy, give rise to a size-dependent assembly of nanoparticles at the interfaces. While the richness of opportunities that arise from this segregation behavior is evident, understanding the parameters that control the self-assembly, the structure and dynamics of the nanoparticles at the interface, the barrier properties of the assembly, and the rate of particle exchange is key to the use of these assemblies for the design and fabrication of devices. Here, a study on the structure of the nanoparticle assembly, using electron microscopy, atomic force microscopy (AFM), and X-ray scattering methods, is presented. In addition, the in-plane dynamics of the particles was investigated by fluorescence photobleaching methods, where the size-dependent fluorescence emission of the nanoparticles provides a direct probe of their spatial distribution. The understanding and thereafter the control over the unique organizations of the nanoparticle assembly at interfaces render the possibility to fabricate functional nanostructured materials with hierarchical orderings, like ultrathin nanoparticle membranes or nanoparticle-decorated breath figures.^{17,18}

Experimental Section

Tri-*n*-octyl-phosphine-oxide (TOPO) covered CdSe nanoparticles were prepared as described in the literature^{19,20} and repeatedly precipitated in methanol to remove most of the TOPO not bound to the nanoparticles. Water droplets with diameters from 10 to 100 microns were obtained by adding water into a

*To whom correspondence should be addressed. E-mail: dinsmore@physics.umass.edu (A.D.D.); tsemrick@mail.pse.umass.edu (T.E.); russell@mail.pse.umass.edu (T.P.R.).

[†] Department of Polymer Science and Engineering, University of Massachusetts.

[‡] Australian Nuclear Science and Technology Organization.

[§] Department of Physics, University of Massachusetts.

(1) Pieranski, P. *Phys. Rev. Lett.* **1980**, *45*, 569.

(2) Binks, B. P.; Clint, J. H. *Langmuir* **2002**, *18*, 1270.

(3) Dinsmore, A. D.; Hsu, M. F.; Nikolaidis, M. G.; Marquez, M.; Bausch, A. R.; Weitz, D. A. *Science* **2002**, *298*, 1006.

(4) Velev, O. D.; Furusawa, K.; Nagayama, K. *Langmuir* **1996**, *12*, 2374.

(5) Binks, B. P.; Lumsdon, S. O. *Langmuir* **2000**, *16*, 8622–8631.

(6) Wong, S. M.; Cha, J. N.; Choi, K. S.; Deming, T. J.; Stucky, G. D. *Nano Lett.* **2002**, *2*, 583–587.

(7) Wang, H.; Hobbie, E. K. *Langmuir* **2003**, *19*, 3091–3093.

(8) Zhai, X.; Efrima, S. *J. Phys. Chem.* **1996**, *100*, 10235–10242.

(9) Schwartz, H.; Harel, Y.; Efrima, S. *Langmuir* **2001**, *17*, 3884–3892.

(10) Brus, L. *Appl. Phys. A* **1991**, *53*, 465.

(11) Alivisatos, A. P. *Science* **1996**, *271*, 933.

(12) Alivisatos, A. P.; Barbara, P. F.; Castleman, A. W.; Chang, J.; Dizon, D. A.; Klein, M. L.; McLendon, G. L.; Miller, J. S.; Ratner, M. A.; Rosky, P. J.; Stupp, S. I.; Thompson, M. E. *Adv. Mater.* **1998**, *10*, 1297.

(13) Lenglet, J.; Bourdon, A.; Bacri, J. C.; Perzynski, R.; Demouchy, G. *Phys. Rev. B* **1996**, *53*, 14941.

(14) Murray, C. B.; Kagan, C. R.; Bawendi, M. G. *Science* **1995**, *270*, 1335–1338.

(15) Redl, F. X.; Cho, K. S.; Murray, C. B.; O'Brien, S. *Nature* **2003**, *423*, 968–971.

(16) Lin, Y.; Skaff, H.; Emrick, T.; Dinsmore, A. D.; Russell, T. P. *Science* **2003**, *299*, 226.

(17) Lin, Y.; Skaff, H.; Böker, A.; Dinsmore, A. D.; Emrick, T.; Russell, T. P. *J. Am. Chem. Soc.* **2003**, *125*, 12690–12691.

(18) Böker, A.; Lin, Y.; Chiapperini, K.; Horowitz, R.; Thompson, M.; Carreon, V.; Xu, T.; Abetz, C.; Skaff, H.; Dinsmore, A. D.; Emrick, T.; Russell, T. P. *Nat. Mater.* **2004**, *3*, 302.

(19) Peng, Z. A.; Peng, X. G. *J. Am. Chem. Soc.* **2001**, *123*, 183.

(20) Skaff, H.; Ilker, M. F.; Coughlin, E. B.; Emrick, T. *J. Am. Chem. Soc.* **2002**, *124*, 5729.

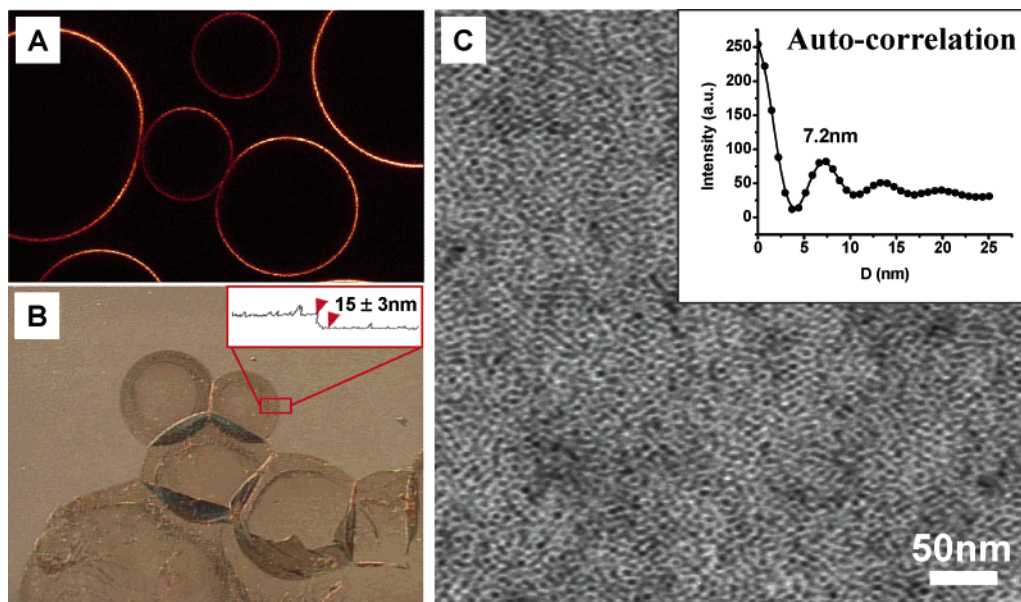


Figure 1. (A) Fluorescence confocal microscope image of water droplets dispersed in toluene, covered with CdSe nanoparticles. (B) Differential interference contrast optical microscopy image of dried droplets on a silicon substrate. Inset: AFM height section analysis. (C) TEM image of a dried droplet. Inset: Autocorrelation function of the TEM image.

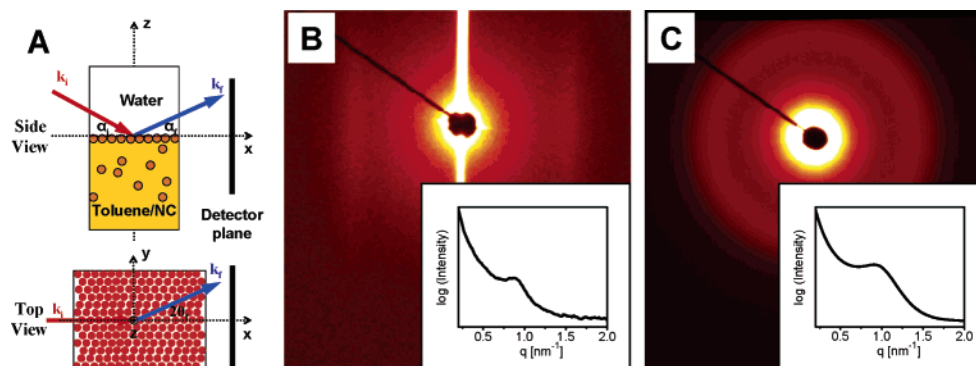


Figure 2. (A) GISAXS experimental setup. (B) GISAXS pattern from nanoparticle assembly at a planar toluene–water interface. The inset depicts an intensity scan along q_y . (C) SAXS pattern from nanoparticle-stabilized water droplets in toluene. The inset shows an azimuthal intensity scan.

dispersion of the nanoparticles in toluene, followed by shaking. The CdSe nanoparticles, dispersed in toluene, assembled at the toluene–water interfaces within seconds, stabilizing the dispersion of the water droplets. Excess nanoparticles in the oil phase were removed by replacing the toluene phase with pure solvent. Fluorescence confocal microscopy studies were performed with a Leica TCS SP2 laser scanning confocal microscope (LSCM) with an oil-emersion objective and Ar-laser excitation. Bright field transmission electron microscopy (TEM) was performed on samples using a JEOL 100CX electron microscope operated at 100 kV. In situ grazing incidence small-angle X-ray scattering (GISAXS) at a planar toluene–water interface and small-angle X-ray scattering (SAXS) on nanoparticle-stabilized water droplets in toluene were performed at the Advanced Photon Source (APS) at the Argonne National Laboratory.

Results and Discussion

Figure 1A shows a fluorescence confocal microscope image of water droplets dispersed in toluene (fluorescence excitation, 488 nm; emission, 610 nm), where the 4.6 nm core diameter CdSe nanoparticles are assembled at the interface. Shown in Figure 1B is an optical microscope image of several nanoparticle-stabilized water droplets that were isolated and dried on a silicon substrate. The toluene and water evaporated, leaving collapsed layers of nanoparticles whose thicknesses were twice the thickness of the shell. Using atomic force microscopy, the thickness

of the nanoparticle assembly was found to be 15 ± 3 nm, approximately twice the diameter of the ligand-covered nanoparticles, indicating that a monolayer of nanoparticles had assembled at the oil–water interface. A similar experiment was performed using a TEM grid, and the electron micrograph shown in Figure 1C was obtained. The autocorrelation function of the TEM image is shown in the inset. No long-range order is observed in the dried nanoparticle assembly. The mean interparticle spacing of 7.2 nm is comparable to the effective diameter of the CdSe core and the organic ligands.

The experimental setup of in situ GISAXS at a planar toluene–water interface is shown in the schematic of Figure 2A. Presented in Figure 2B is a GISAXS pattern where distinct off-specular reflections are seen, along with a strong specular reflection. The off-specular scattering consists of two Bragg rods oriented normal to the toluene–water interface, which is characteristic of a monolayer of spheres assembled at the interface. The maximum in the scattering rods occurs at $q_y = 0.91 \text{ nm}^{-1}$, corresponding to a spacing of ~ 7 nm which is commensurate with the core diameter of the nanoparticles plus twice the length of the stabilizing ligand. Comparison of the measured GISAXS patterns with model calculations²¹ indicates that

(21) Lazzari, R. *J. Appl. Crystallogr.* **2002**, *35*, 406–421.

the assembly is liquid-like with no long-range order. The combination of microscopy and scattering data reveals that the nanoparticles assemble at the oil–water interface as a monolayer, but the packing of the particles is liquid-like, exhibiting no long-range order. SAXS data on the assembly of nanoparticles at the surfaces of water droplets are shown in Figure 2C. A diffuse maximum in the isotropic scattering pattern is seen at $q = 0.92 \text{ nm}^{-1}$ with a full width at half-maximum (fwhm) of 0.44 nm^{-1} , indicating a lack of long-range order. These data are consistent with the results on the planar interface, revealing that the packing of the nanoparticles is the same in both cases. The absence of crystalline order is, more than likely, due to the polydispersity in the size of the nanoparticles,²² which is a few percent of the average diameter.

Assembly of the particles is driven by the minimization of the Helmholtz free energy. Based on the arguments of Pieranski,¹ the change in the interfacial energy due to the placement of a single particle at the oil–water interface is given by

$$\Delta E = -\frac{\pi R^2}{\gamma_{O/W}}(\gamma_{O/W} - \gamma_{P/W} + \gamma_{P/O})^2$$

when $\gamma_{O/W} > |\gamma_{P/W} - \gamma_{P/O}|$ (no adsorption when this condition is not satisfied). The three contributions to the changes in the interfacial energy are the particle/oil interfacial energy ($\gamma_{P/O}$), the particle/water interfacial energy ($\gamma_{P/W}$), and the oil/water interfacial energy ($\gamma_{O/W}$). Based on published values²³ of $\gamma_{O/W} = 35.7 \text{ mN/m}$ and estimates of $\gamma_{P/O} \sim 15 \text{ mN/m}$ and $\gamma_{P/W} \sim 40 \text{ mN/m}$, $\Delta E \sim -5k_B T$ and $-10k_B T$ for 2.7 and 4.6 nm core diameter nanoparticles, respectively. The weak energy associated with placing the nanoparticles at the interface gives rise to a thermally activated escape from the interface. The desorption of particles from the interface is expected to be exponential in time, with a characteristic time, τ_{off} , that should increase with the adsorption free energy, ΔE , as $\tau_{\text{off}} = A \exp(-\Delta E/k_B T)$, with A depending only weakly on size. Because $\Delta E \propto R^2$, the residence time of the nanoparticles at the interface increases with increasing particle size. Qualitatively, the adsorption of nanoparticles at the interface shows a clear size-dependence. Droplets with 4.6 nm particles assembled at the interface are stable for days in pure toluene, while the droplets with 2.7 nm particles coalesce within hours owing to a reduced surface coverage by desorption. No droplet stabilization is seen for particles with diameters less than $\sim 1.6 \text{ nm}$, suggesting that thermal fluctuations reduce the concentration of adsorbed particles below the level needed to form a stable interface.

To probe the size-dependent assembly of nanoparticles at interfaces more quantitatively, mixtures of two different sized nanoparticles were investigated. A blend of 2.7 and 4.6 nm diameter nanoparticles was prepared and allowed to assemble on the surface of water droplets by shaking. Subsequently the time dependence of the ratio of peak emission intensities of the two different sized particles at the interface was monitored. The 2.7 nm particles fluoresce at 525 nm, whereas the 4.6 nm diameter particles fluoresce at 610 nm. Gaussian profiles were used to deconvolute the two emission profiles. The background fluorescence from the nanoparticles in the oil phase and in the same focal plane was used to normalize the data so as to

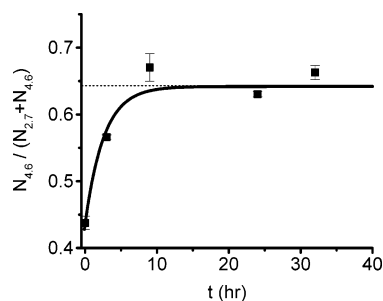


Figure 3. Time dependence of the relative portion of the 4.6 nm particles in a mixture with 2.7 nm particles at the interface. The solid line shows a fit to an exponential with characteristic time $\tau = 8.6(\pm 3) \times 10^3 \text{ s}$.

compensate for the depth-dependence of the fluorescence intensity (the inner filter effect).²⁴ Figure 3 shows that the relative concentration of 4.6 nm particles assembled at the interface increases approximately exponentially with time at the early stage of displacement when a simple exchange process dominates. The characteristic time for this exchange process is $8.6(\pm 3) \times 10^3 \text{ s}$. The spontaneous escape of the 2.7 nm nanoparticles is consistent with $\Delta E \sim -5k_B T$. After $\sim 24 \text{ h}$, the two different sized particles were seen to undergo a phase separation at the interface, as reported earlier.¹⁶ After 48 h, circular areas of the 4.6 nm particles are seen to form on the droplet surface. This two-dimensional phase separation of the nanoparticles at the interface requires an in-plane mobility that can be quantified in terms of a diffusion coefficient. The observed nonfaceted shape of the large-particle domain supports the previous conclusion that the nanoparticle assembly is liquid-like.

The in-plane diffusion of nanoparticles assembled at interfaces in an equilibrated system was studied using fluorescence recovery after photobleaching^{25–27} (FRAP) and fluorescence loss in photobleaching (FLIP). In the FRAP experiments, the nanoparticles assembled at the interface were photobleached at the focal point of the laser beam (Ar^+ laser, 488 nm line) at a high power for 10 s. The subsequent diffusion of the surrounding nonbleached nanoparticles into the bleached area leads to a recovery of the fluorescence, which is measured using a laser at lower power. While the diffusion of different sized particles could be measured, the mobility of the 4.6 nm nanoparticles was chosen since the escape of these particles from the interface is much longer than the time scale of photobleaching experiments ($< 1 \text{ h}$). The normalized recovery curves from the bleached spot were analyzed by fitting the data to^{25–27}

$$F(t) = \sum_{n=0}^{\infty} \frac{(-\kappa)^n}{n!} \frac{1}{1 + n \left[1 + \left(\frac{2t}{\tau_D} \right) \right]}$$

where κ is a bleaching constant that depends on the sensitivity of the system for bleaching. τ_D (the characteristic 2-D diffusion time) is related to the 2-D diffusion coefficient by $\tau_D = w^2/4D$, where w is the radius of the waist of the focused laser beam, i.e., the radius at which

(24) van Oostveldt, P.; Bauwens, S. *J. Microsc.* **1990**, *158*, 121–132.

(25) Axelrod, D.; Koppel, D. E.; Schlessinger, J.; Elson, E.; Webb, W. W. *Biophys. J.* **1976**, *16*, 1055.

(26) Blonk, J. C. G.; Don, A.; Aalst, H. V.; Birmingham, J. J. *J. Microsc.* **1993**, *169*, 363.

(27) Icenogle, R. D. *Biopolymers* **1983**, *22*, 1919–1948.

(22) Collier, C. P.; Vossmeier, T.; Heath, J. R. *Annu. Rev. Phys. Chem.* **1998**, *49*, 371.

(23) Birdi, K. S.; Vu, D. T. *Handbook of Surface and Colloid Chemistry*; CRC Press: Boca Raton, 1997.

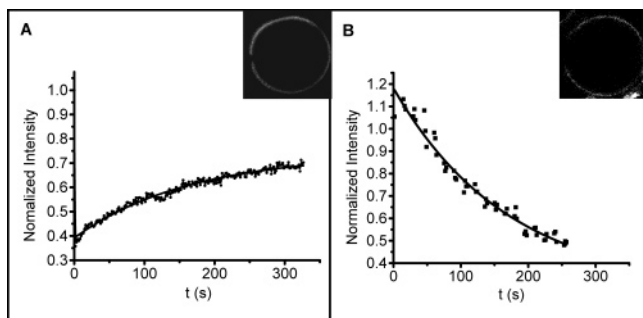


Figure 4. (A) FRAP and (B) FLIP experiments on an assembly of 4.6 nm nanoparticles at toluene–water interfaces. Inset: LSCM image of the droplets being bleached. The intensity is normalized by the average value before bleaching.

the intensity falls to e^{-2} of the maximum intensity. This model is valid for the idealized case of pure 2-D diffusion that is monitored by a laser beam with a Gaussian intensity profile. The profile of the laser beam was obtained by point-bleaching a fluorescently labeled thin polystyrene film under experimental conditions identical to that used in the nanoparticle experiments. The beam waist, w , was measured to be $3 \mu\text{m}$. A typical recovery measurement and fit to the data are shown in Figure 4A where the fluorescence image of the cross section of a droplet is shown (the dark region in the ring has been bleached). From these, D can be calculated to be $1.3(\pm 0.3) \times 10^{-10} \text{ cm}^2/\text{s}$.

In the FLIP experiments, a circular area at the interface was repeatedly bleached at a high laser power. The reduction of the fluorescence intensity from the unbleached area was then measured as a function of time, using a reduced laser power. Multiple regions equidistant from the bleaching area were probed to increase precision. The measured areas were chosen far enough from the bleached area to avoid any direct bleaching from the laser beam profile. To ensure that there was no generalized bleaching effect due to the imaging, the fluorescence emission intensity from at least one neighboring unbleached droplet, included in the field of view, was used for normalization. Shown in Figure 4B is a typical measurement of the fluorescence loss at the droplet interface as a function of time. At long time, the intensity within a few microns of the bleaching area has decreased to near background levels, showing that a lateral diffusion on the droplet

surface has occurred. The effective 2-D diffusion coefficient D obtained from fits to these measurements was $3.3(\pm 0.7) \times 10^{-10} \text{ cm}^2/\text{s}$.

Both the FRAP and FLIP measurements show that the nanoparticles are mobile in the plane of the interface. For the 4.6 nm nanoparticles, the in-plane diffusion coefficient is 4 orders of magnitude lower than the diffusion coefficient of nanoparticles dispersed in toluene, as measured by dynamic light scattering. Since the equator of the droplet was chosen as the focal plane, the bleaching point is extended in the z direction that could lead to slight errors in the evaluation of the diffusion. Nonetheless, the mobility of the particles and the reduction in the diffusion coefficient due to the confinement of the nanoparticles to the interface are clear.

Conclusion

In summary, it has been shown that nanoparticles assemble at the interface of two immiscible liquids as a disordered but densely packed monolayer. In addition, a size-dependent exchange of particles occurs, where larger particles displace the smaller particles at a rate that is consistent with their adsorption energies. The in-plane dynamics of the nanoparticles was investigated in situ by fluorescence photobleaching methods, making use of the inherent fluorescence emission from the nanoparticles. The in-plane diffusion coefficient of the nanoparticles was found to be 4 orders slower than that of the particles in solution. The results presented here have implications in the design of hierarchical self-assemblies of nanoparticles for the one-step fabrication of devices on multiple length scales.

Acknowledgment. This work was supported by the Department of Energy, Office of Basic Energy Science, the Max Kade Foundation, and the National Science Foundation supported Materials Research Science and Engineering Center. ChemMatCARS Sector 15 is principally supported by the National Science Foundation/Department of Energy under Grant Number CHE0087817 and by the Illinois board of higher education. The Advanced Photon Source is supported by the U.S. Department of Energy, Basic Energy Sciences, Office of Science, under Contract No. W-31-109-Eng-38.

LA048000Q